inorganics

MDPI

Article

Synthesis and Evaluation of ^{99m}Tc-Tricabonyl Labeled Isonitrile Conjugates for Prostate-Specific Membrane Antigen (PSMA) Image

Nadeem Ahmed Lodhi [1,2], Ji Yong Park [1,3], Kyuwan Kim [3], Mi Kyung Hong [1,4], Young Joo Kim [1,4], Yun-Sang Lee [1,3], Gi Jeong Cheon [1], Keon Wook Kang [1,3,4] and Jae Min Jeong [1,3,4,*]

1 Department of Nuclear Medicine, Seoul National University College of Medicine, Seoul 03080, Korea; nadiimlodhi@gmail.com (N.A.L.); pjypoo@hanmail.net (J.Y.P.); mkhong@snuh.org (M.K.H.); yjukim@snu.ac.kr (Y.J.K.); wonza43@snu.ac.kr (Y.-S.L.); larrycheon@gmail.com (G.J.C.); kangkw@snu.ac.kr (K.W.K.)

2 Isotope Production Division, Pakistan Institute of Nuclear Science & Technology (PINSTECH), P. O, Nilore, Islamabad 45650, Pakistan

3 Department of Biomedical Sciences, Seoul National University Graduate School, Seoul 03080, Korea; kwkim0111@gmail.com

4 Cancer Research Institute, Seoul National University, Seoul 03080, Korea

* Correspondence: jmjng@snu.ac.kr; Tel.: +82-2-2072-3805; Fax: +82-2-766-9083

Received: 7 December 2019; Accepted: 9 January 2020; Published: 14 January 2020

Abstract: Prostate-specific membrane antigen (PSMA) is a biomarker expressed on the surface of prostate cancer (PCa). In an effort to improve the detection and treatment of PCa, small urea-based PSMA inhibitors have been studied extensively. In the present study, we aimed to develop ^{99m}Tc-tricabonyl labeled urea-based PSMA conjugates containing isonitrile (CN-R)-coordinating ligands ([^{99m}Tc]Tc-**15** and [^{99m}Tc]Tc-**16**). Both the PSMA conjugates were obtained at high radiochemical efficiency (≥98.5%). High in vitro binding affinity was observed for [^{99m}Tc]Tc-**15** and [^{99m}Tc]Tc-**16** (K_d = 5.5 and 0.2 nM, respectively) in PSMA-expressing 22Rv1 cells. Tumor xenografts were conducted using 22Rv1 cells and rapid accumulation of [^{99m}Tc]Tc-**16** (1.87 ± 0.11% ID/g) was observed at 1 h post-injection, which subsequently increased to (2.83 ± 0.26% ID/g) at 4 h post-injection. However, [^{99m}Tc]Tc-**15** showed moderate tumor uptake (1.48 ± 0.18% ID/g), which decreased at 4 h post-injection (0.81 ± 0.09% ID/g). [^{99m}Tc]Tc-**16** was excreted from non-targeted tissues with high tumor-to-blood (17:1) and tumor-to-muscle ratio (41:1) at 4 h post-injection at approximately 4 times higher levels than [^{99m}Tc]Tc-**15**. Uptakes of [^{99m}Tc]Tc-**15** and [^{99m}Tc]Tc-**16** to PSMA-expressing tumor and tissues were significantly blocked by co-injection of 2-(Phosphonomethyl)-pentandioic acid (2-PMPA), suggesting that their uptakes are mediated by PSMA specifically. Whole-body single photon emission computed tomography imaging of [^{99m}Tc]Tc-**16** verified the ex vivo biodistribution results and demonstrated clear visualization of tumors and tissues expressing PSMA compared to [^{99m}Tc]Tc-**15**. In conclusion, using [^{99m}Tc]Tc-**16** rather than [^{99m}Tc]Tc-**15** may be the preferable because of its relatively high tumor uptake and retention.

Keywords: prostate cancer; prostate-specific membrane antigen; Technetium-99m; SPECT; Isonitrile

1. Introduction

Prostate cancer (PCa) is a commonly diagnosed disease and is the second leading cause of cancer death in the United States. In 2018, approximately 164,690 men were diagnosed with PCa, leading to an estimated 29,430 deaths [1]. Prostate-specific membrane antigen (PSMA) is glutamate carboxypeptidase

II (GCPII) or *N*-acetyl-L-aspartyl-L-glutamate peptidase I (NAALADase I), and is a type II integral transmembrane glycoprotein (100–120 kDa). PSMA is expressed in most PCa tissues and its expression often increased in metastatic, poorly differentiated, androgen-independent, and hormone-refractory carcinoma [2–4]. In addition, the levels of PSMA expression correlate with the progression, stage, and the risk of disease [5,6]. Therefore, PSMA is considered to be a promising, reliable, and an efficient biomarker for PCa imaging and therapeutic application.

PSMA was originally imaged by FDA approved ^{111}In-labeled monoclonal antibody (^{111}In-capromab pendetide, ProstaScint®) to diagnose PCa [7–10]. However, it binds to an intracellular site of PSMA and is only able to access necrotic tumor cells [11,12]. Therefore, it failed to gain wide acceptance in the field of nuclear medicine. Subsequently, a humanized monoclonal antibody (J591) to target the extracellular domain of the PSMA was evaluated preclinically as an imaging and radioimmunotherapeutic agent [13–16]. Despite improved target efficiency, its slow pharmacokinetics and slow clearance from non-target tissue made it incompatible for diagnostic applications. Thereafter, small molecular weight ligands, mainly urea-based small molecules, showed promising applications for imaging PSMA-expressing prostate tumor xenografts owing to their rapid clearance from the non-target tissue and very high tumor-to-background ratio [17,18]. Recently, numerous urea-based PSMA ligands have been developed to improve the affinity, specificity, and targeting efficacy of diagnostic agents [19–28]. Several molecules have been tested in preclinical and clinical stages for the visualization of primary, metastatic bone, and soft-tissue lesions of PCa [29–32].

Technetium-99m (^{99m}Tc) is the most widely used radionuclide for single photon emission computed tomography (SPECT) because of its excellent nuclear physical characteristics ($t_{1/2}$ = 6 h, $E\gamma$ = 140 keV). It is conveniently available from ^{99}Mo/^{99m}Tc generator in high specific activity [33]. There was a report of ^{99m}Tc-labeled urea-based PSMA ligand for PCa imaging [34]. A bifunctional chelating agent used for this compound was a tripeptide containing cysteine moiety which is somewhat vulnerable to air and forms a monodentate complex. Thus we tried to find a more advanced method for the ^{99m}Tc-labeling which leads to multidentate complex with increased affinity.

The $[^{99m}Tc][Tc(CO)_3(H_2O)_3]^+$ has emerged as a versatile core for the labeling of biomolecules because of its excellent chelation chemistry, chemical inertness, and thermodynamic stability [35–37]. Furthermore, suitable mono-, bi-, and tri-dentate ligand can easily be coordinated with a $[^{99m}Tc][Tc(CO)_3(H_2O)_3]^+$ core at elevated temperature (>90 °C) by replacement of three water molecule in aqueous solution [38,39].

^{99m}Tc-labeled hexakis-methoxyisobutylisonitrile (^{99m}Tc-MIBI) is a lipophilic complex with a positive charge and is a well-known myocardial perfusion SPECT agent in the clinical field [40,41]. In the ^{99m}Tc-MIBI complex, ^{99m}Tc(I) is a soft metal and is complexed by six soft isonitrile ligands in a hexavalent fashion to form a stable octahedral complex [42]. The metal center of $[^{99m}Tc][Tc(CO)_3(H_2O)_3]^+$ is likewise soft and the isonitrile ligands can strongly coordinate with it in a 3:1 ratio, as reported previously [43–45]. Isonitrile derivatives of arginine-glycine-aspartate (RGD) and nitroimidazole were labeled with ^{99m}Tc by inducing a reaction with $[^{99m}Tc][Tc(CO)_3(H_2O)_3]^+$ and have been evaluated in vivo with promising results [38,46]. Recently, a ^{99m}Tc-labeled tris-folate conjugate was developed by using isonitrile and $[^{99m}Tc][Tc(CO)_3(H_2O)_3]^+$ to target folate receptors [47].

Here, we tried to develop an asymmetrical urea-based PSMA using the isonitrile containing vectors **15** and **16** with two different spacers. Both of these were labeled with ^{99m}Tc in a trivalent fashion using $[^{99m}Tc][Tc(CO)_3(H_2O)_3]^+$. ^{99m}Tc-labeled PSMA conjugates $[^{99m}Tc]$Tc-**15** and $[^{99m}Tc]$Tc-**16** were then tested in vitro for their specific PSMA binding as well as in vivo uptake in a prostate cancer 22Rv1 xenograft model as potential PSMA imaging agents.

2. Results

2.1. Chemistry

Asymmetrical urea **1** was synthesized by treating L-glutamic acid di-*tert*-butyl ester hydrochloride with triphosgene in the presence of triethylamine (TEA) at −78 °C to produce an intermediate isocyanate, which subsequently was treated with *N*′-Cbz-L-lysine *tert*-butyl ester to produce **1** after purification by silica gel chromatography (Scheme 1). The carbobenzoxy (Cbz) protecting group was removed by catalytic hydrogenation to produce **2** in quantitative yield, and subsequently reacted with Fmoc-6-Ahx–OH in the presence of a coupling agent (HBTU) to produce **3**. Selective removal of the Fmoc group (20% piperidine/*N*,*N*-dimethylformamide (DMF)) produce **4**, and the *tert*-butyl protecting group was then removed to yield **5**, which was used for the synthesis of the PSMA conjugate **15**.

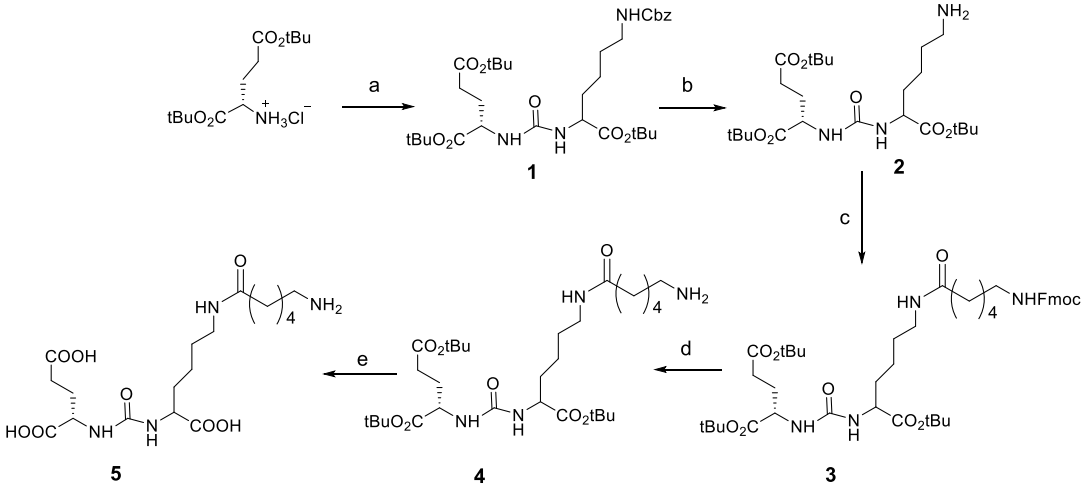

Scheme 1. Reagents and conditions: (**a**) Lys(Cbz)-OtBu, triphosgene, −78 °C–RT, 18 h; (**b**) 10% Pd/C, methanol, 18 h; (**c**) Fmoc-6-Ahx–OH, *N*,*N*,*N*′,*N*′-Tetramethyl-*O*-(1*H*-benzotriazol-1-yl)uronium hexafluorophosphate (HBTU), *N*,*N*-diisopropylethylamine (DIPEA), 0 °C–RT, overnight; (**d**) 20% piperidine/*N*,*N*-dimethylformamide (DMF), 1 h; (**e**) trifluoroacetic acid (TFA): dichloromethane (DCM) (1:1), 18 h.

For the synthesis of the PSMA conjugate **16**, **4** was conjugated with Fmoc–Phe–OH using HBTU to generate compound **6** (Scheme 2). Selective deprotection of Fmoc group from **6** using 20% piperidine/DMF produced **7**. An additional conjugation of the Fmoc–Phe–OH group to **7**, followed by removing the Fmoc group generated **9**. Compound **9** was then treated with 6-Boc-aminohexanoic acid in the presence of a coupling agent (HBTU) to produce **10.** Subsequently, Boc and *tert*-butyl groups were removed using a mixture of trifluoroacetic acid (TFA)/dichloromethane (DCM) (1:1 *v*/*v*) to generate compound **11**.

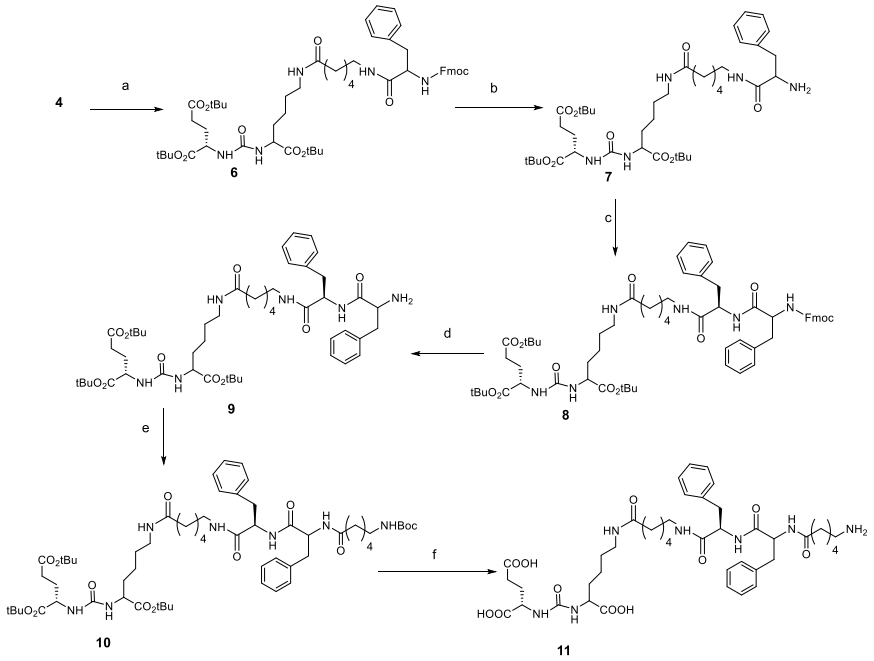

Scheme 2. Reagents and conditions: (**a**) Fmoc-Phe-OH, HBTU, DIPEA, 0 °C–RT overnight; (**b**) 20% piperidine/DMF, 1 h; (**c**) Fmoc-Phe-OH, HBTU, DIPEA, 0 °C–RT overnight; (**d**) 20% piperidine/DMF, 1 h; (**e**) Boc-6-Ahx–OH, HBTU, DIPEA, 0 °C–RT overnight; (**f**) TFA:DCM (1:1, *v*/*v*).

Synthesis of TFP-activated isonitrile and conjugation with **5** and **11** was accomplished in four steps (Scheme 3). First, *N*-formyl-β-alanine (**12**) was obtained by refluxing a mixture of β-alanine, formic acid, and acetic anhydride. The carboxylic acid group was activated with TFP to produce **13**. The formyl group was converted to isonitrile with a dehydrating agent triphosgene to generate **14**. Finally, isonitrile was conjugated to **5** or **11** in the presence of *N*,*N*-diisopropylethylamine (DIPEA) to produce the final PSMA conjugates **15** and **16**. The final products were purified by prep-HPLC. The identities of intermediate compounds and final precursors were confirmed by ^{1}H-NMR and ESI/MS.

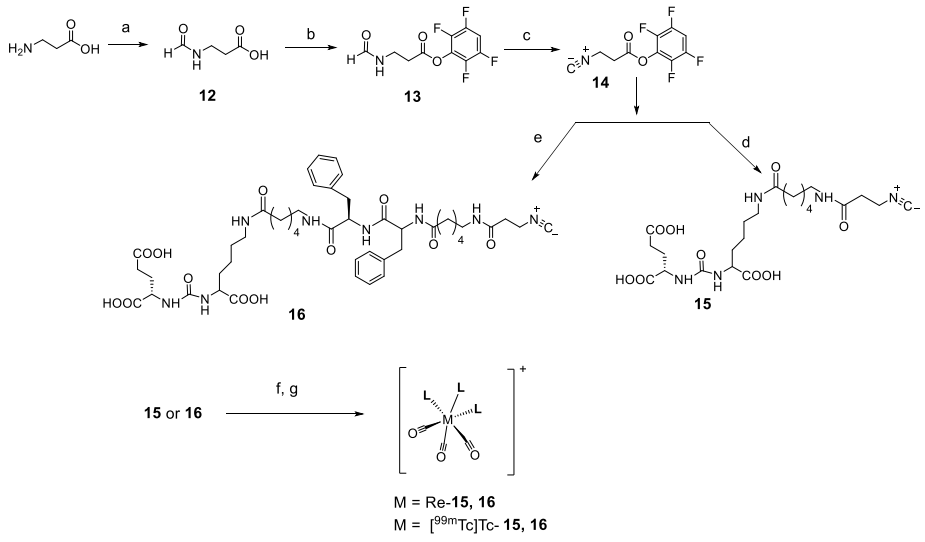

Scheme 3. Reagents and conditions: (**a**) formic acid, acetic anhydride, refluxed, 3 h; (**b**) 2,3,5,6-tetrafluorophenol, *N*,*N*′-dicyclohexylcarodiimide (DCC), DMF, RT, 24 h; (**c**) triphosgene, DCM, TEA, 0 °C, 1.5 h; (**d**) 5,DIPEA, RT, 5 h; (**e**) 10, DIPEA, RT, 5 h; (**f**) $[Re(CO)_3(H_2O)_3]Br$; (**g**) $[^{99m}Tc]Tc(H_2O)_3(CO)_3]^+$.

2.2. Radiolabeling

[^{99m}Tc][Tc(I)$(OH_2)_3(CO)_3$]$^+$ was prepared at ≥98.5% radiolabeling efficiency (Figure 1A). Under the given conditions, [^{99m}Tc]Tc-**15** and [^{99m}Tc]Tc-**16** were consistently obtained at high radiolabeling efficiency (≥98.5%). Subsequent purification by radio-HPLC provided high radiochemical purity (≥99.5%) of [^{99m}Tc]Tc-**15** and [^{99m}Tc]Tc-**16** (Figure 1B,C). Molar activities of both labeled products were 4.07×10^8 GBq/mol.

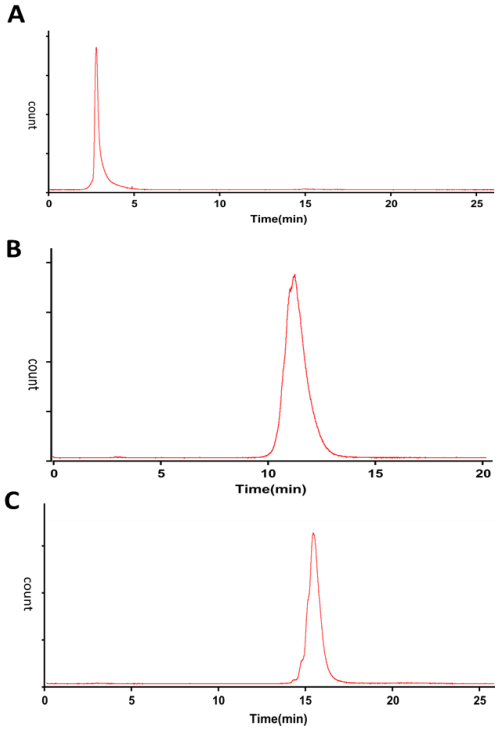

Figure 1. Radio-HPLC profile of (**A**) [^{99m}Tc]Tc$(H_2O)_3(CO)_3]^+$, (**B**) [^{99m}Tc]Tc-**15,** and (**C**) [^{99m}Tc]Tc-**16** by gradient methods **5** and **6,** radiochemical purity >98.5%.

2.3. In Vitro Serum Stability and Distribution Coefficient (LogD)

In vitro stability of [^{99m}Tc]Tc-**15** and [^{99m}Tc]Tc-**16** were tested in human serum at 37 °C, and both showed high stability at least for 6 h (Figure 2). LogD values were determined by partitioning [^{99m}Tc]Tc-**15** or [^{99m}Tc]Tc-**16** between 1-octanol and PBS (pH 7.4) and found to be −3.72 ± 0.05 and −2.10 ± 0.03, respectively, indicating high hydrophilicity of the compounds.

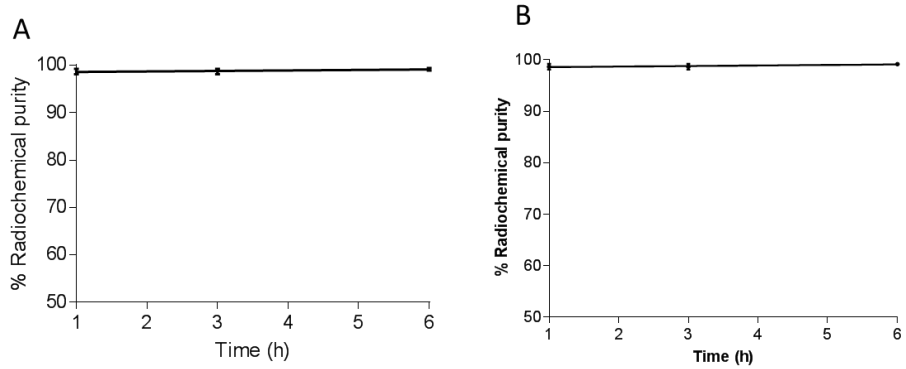

Figure 2. In vitro stability in human serum at 1, 3, and 6 h incubation at 37 °C determined by thin layer chromatography (TLC)-SG developed with methanol and HCl (99: 1; *v*/*v*) and radio-HPLC for (**A**) [^{99m}Tc]Tc-**15** and (**B**) [^{99m}Tc]Tc-**16**.

2.4. In Vitro Binding Affinity (K_d)

Saturation binding analysis was conducted to determine the binding affinity of [^{99m}Tc]Tc-**15** or [^{99m}Tc]Tc-**16** using 22Rv1 cells. Specific binding was determined by subtracting total binding from non-specific binding obtained by blocking with 2-(Phosphonomethyl)-pentandioic acid (2-PMPA) (250 μM). The binding affinity K_d values of [^{99m}Tc]Tc-**15** and [^{99m}Tc]Tc-**16** were determined by nonlinear regression to be 5.5 ± 0.99 and 0.2 ± 0.01 nM, respectively.

2.5. Ex Vivo Biodistribution

Ex vivo biodistribution studies of [^{99m}Tc]Tc-**15** and [^{99m}Tc]Tc-**16** were performed at 1 and 4 h post-tail vein injection in 22Rv1 tumor bearing BALB/c male mice (Tables 1 and 2). [^{99m}Tc]Tc-**15** and [^{99m}Tc]Tc-**16** showed tumor uptakes of 1.48 ± 0.18 and 1.87 ± 0.11% ID/g at 1 h post-injection, respectively. At 4 h post-injection, significantly decreased tumor uptake was observed for [^{99m}Tc]Tc-**15** (0.81 ± 0.09% ID/g) ($p < 0.01$), whereas [^{99m}Tc]Tc-**16** showed significantly increased in tumor uptake (2.83 ± 0.26% ID/g) ($p < 0.01$). As expected, the highest accumulation of activity for ^{99m}Tc-labeled conjugates were observed in the kidney (59.59 ± 8.45% ID/g for [^{99m}Tc]Tc-**15** and 24.66 ± 2.17% ID/g for [^{99m}Tc]Tc-**16**) at 1 h post-injection. However, at 4 h post-injection the kidney uptake for [^{99m}Tc]Tc-**15** decreased (13.72 ± 5.45% ID/g), whereas [^{99m}Tc]Tc-**16** showed increased kidney uptake (39.65 ± 6.86% ID/g). Furthermore, [^{99m}Tc]Tc-**15** showed lower splenic uptake at all-time points compared to [^{99m}Tc]Tc-**16**. In the blocking study, all of the tumor uptakes were reduced to background levels by co-injection of 2-PMPA. In addition, kidney uptake dramatically reduced: 4.22 ± 1.30 and 1.44 ± 0.09%ID/g for [^{99m}Tc]Tc-**15** at 1 and 4 h, respectively, and 5.66 ± 0.6 and 3.59 ± 0.52% ID/g for [^{99m}Tc]Tc-**16** at 1 and 4 h, respectively. Uptake in the liver was relatively low for both ^{99m}Tc-labeled conjugates and was further decreased at 4 h post-injection.

Table 1. Biodistribution and uptake ratios of [^{99m}Tc]Tc-**15** prostate-specific membrane antigen (PSMA)-targeted 22Rv1 tumor bearing BALB/c male nude mice at 1 and 4 h.

Tissues	1 h	4 h	1 h Blockade	4 h Blockade
Blood	0.60 ± 0.02	0.31 ± 0.02	0.52 ± 0.09	0.31 ± 0.01
Muscle	0.17 ± 0.07	0.08 ± 0.01	0.11 ± 0.02	0.08 ± 0.01
Tumor	1.48 ± 0.18 ***	0.81 ± 0.09 ***	0.38 ± 0.12	0.20 ± 0.04
Heart	0.22 ± 0.02	0.12 ± 0.01	0.16 ± 0.03	0.10 ± 0.01
Lung	0.64 ± 0.02	0.30 ± 0.04	0.61 ± 0.20	0.30 ± 0.05
Liver	0.94 ± 0.05	0.85 ± 0.05	0.84 ± 0.12	0.84 ± 0.03
Spleen	0.90 ± 0.14	0.26 ± 0.06	0.15 ± 0.03	0.16 ± 0.01
Stomach	0.31 ± 0.07	0.15 ± 0.02	0.17 ± 0.04	0.14 ± 0.01
Intestine	0.78 ± 0.07	0.81 ± 0.19	0.55 ± 0.13	0.97 ± 0.20
Kidney	59.59 ± 8.45 ***	13.72 ± 5.45 **	4.22 ± 1.30	1.44 ± 009
Bone	0.34 ± 0.02	0.16 ± 0.03	0.26 ± 0.07	0.20 ± 0.03
Tumor/blood	2.50 ± 0.18 ***	2.6 ± 0.13 ***	0.73 ± 0.18	0.65 ± 0.13
Tumor/muscle	8.50 ± 2.80 **	10.4 ± 0.77 ***	3.5 ± 0.50	2.71 ± 0.78
Tumor/liver	1.57 ± 0.15 **	0.96 ± 0.13 **	0.45 ± 0.10	0.24 ± 0.04
Tumor/kidney	0.02 ± 0.00	0.06 ± 0.02	0.09 ± 0.02	0.14 ± 0.03

Results are expressed as % ID/g (mean ± SD for $n = 3$). The blocking studied were performed by co-injection of 2-PMPA (100 μg). *** $p \leq 0.001$, ** $p \leq 0.01$.

Table 2. Biodistribution and uptake ratios of [^{99m}Tc]Tc-**16** in PSMA-targeted 22Rv1 tumor bearing BALB/c male nude mice at 1 and 4 h post-injection.

Tissues	1 h	4 h	1 h Blockade	4 h Blockade
Blood	0.42 ± 0.01	0.17 ± 0.03	0.75 ± 0.08	0.15 ± 0.01
Muscle	0.13 ± 0.02	0.07 ± 0.01	0.22 ± 0.06	0.05 ± 0.01
Tumor	1.87 ± 0.11 ***	2.83 ± 0.26 ***	0.45 ± 0.02	0.39 ± 0.03
Heart	0.36 ± 0.01	0.25 ± 0.05	0.48 ± 0.05	0.11 ± 0.01
Lung	0.52 ± 0.05	0.36 ± 0.04	1.63 ± 0.10	0.45 ± 0.04
Liver	1.17 ± 0.04	0.69 ± 0.11	1.95 ± 0.07	1.33 ± 0.15
Spleen	3.40 ± 0.93	3.44 ± 0.23	0.40 ± 0.03	0.20 ± 0.04
Stomach	0.85 ± 0.23	0.42 ± 0.04	1.04 ± 0.26	0.23 ± 0.04
Intestine	0.47 ± 0.06	1.48 ± 0.18	0.85 ± 0.07	1.26 ± 0.14
Kidney	24.66 ± 2.17 **	39.65 ± 6.86 ***	5.66 ± 0.63	3.59 ± 0.52
Bone	0.63 ± 0.03	1.04 ± 0.15	1.16 ± 0.08	0.47 ± 0.12
Tumor/blood	4.43 ± 0.39 ***	16.70 ± 1.36 ***	0.61 ± 0.07	2.67 ± 0.25
Tumor/muscle	14.05 ± 1.78 ***	40.43 ± 3.97 ***	2.16 ± 0.43	8.44 ± 1.52
Tumor/liver	1.60 ± 0.13 ***	4.17 ± 0.36 ***	0.23 ± 0.02	0.30 ± 0.04
Tumor/kidney	0.08 ± 0.01	0.07 ± 0.01	0.08 ± 0.01	0.11 ± 0.01

Results are expressed as % ID/g (mean ± SD for $n = 4$). The blocking studied were performed by co-injection of 2-PMPA (100 µg). *** $p \leq 0.001$, ** $p \leq 0.01$.

2.6. SPECT Imaging

In order to further validate the capability of [^{99m}Tc]Tc-**15** and [^{99m}Tc]Tc-**16** to target PSMA in vivo, whole-body SPECT/CT imaging in 22Rv1 tumor-bearing BALB/c male nude mice was conducted (Figures 3 and 4). [^{99m}Tc]Tc-**15** and [^{99m}Tc]Tc-**16** were rapidly excreted through the kidneys. [^{99m}Tc]Tc-**15** showed slightly increased uptake in tumors, whereas [^{99m}Tc]Tc-**16** showed a higher tumor to background contrast. The tumor uptake was completely blocked by co-injection of 2-PMPA (Figures 3 and 4).

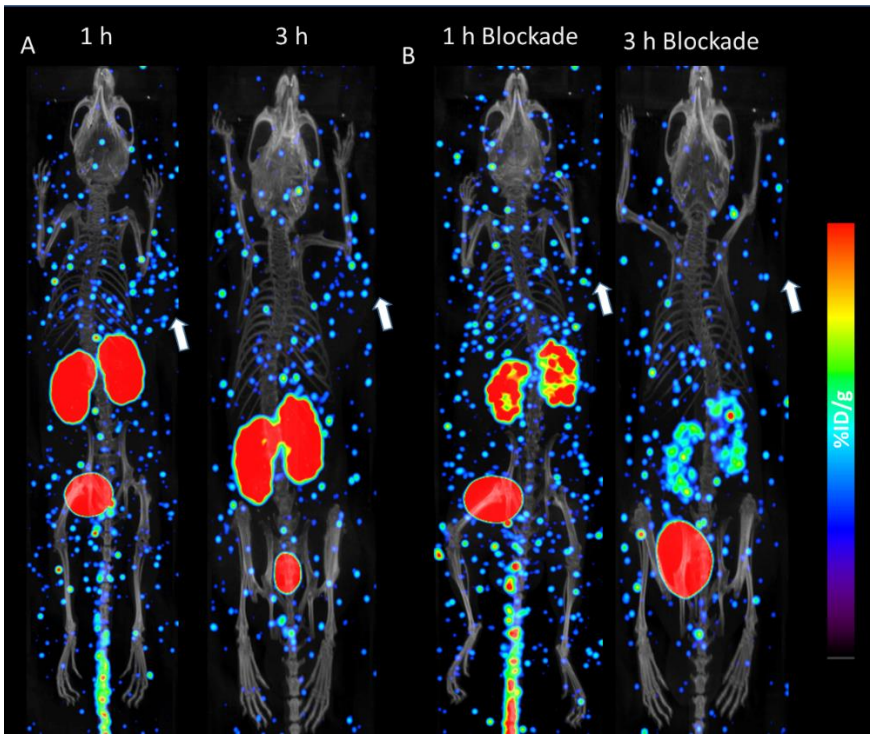

Figure 3. Whole-body SPECT/CT image of [^{99m}Tc]Tc-15 in PSMA-targeted 22Rv1 tumor bearing mice at 1 and 3 h post-injection. (**A**) [^{99m}Tc]Tc-**15** alone. (**B**) Blockade by co-injection of 2-PMPA (100 µg).

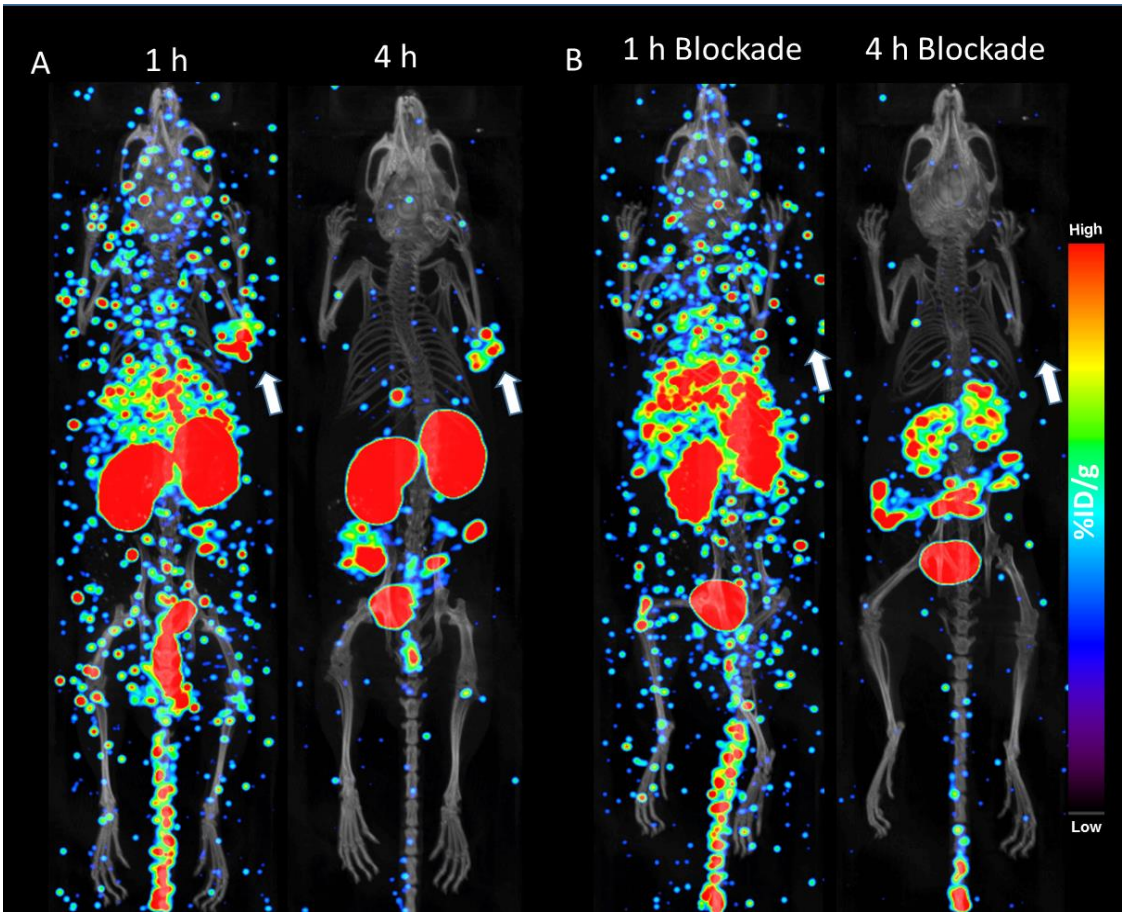

Figure 4. Whole-body SPECT/CT image of [^{99m}Tc]Tc-**16** in PSMA-targeted 22Rv1 tumor bearing mice at 1 and 4 h post-injection. (**A**) [^{99m}Tc]Tc-**16** alone. (**B**) Blockade by co-injection of 2-PMPA (100 μg).

3. Discussion

PSMA is expressed in wide variety of PCa and its expression is correlated with disease stage and plays an important role in early detection of PSMA-positive lesion in patients. It has been reported that the glutamate moiety on urea-based PSMA inhibitors interacts with the S1 binding pocket, which can interact with lipophilic spacers. The S1 binding pocket is a funnel-shaped tunnel with a depth of approximately 20 Å and a width of 8–9 Å [48–50]. The synergistic effect of a glutamate motif and a lipophilic spacer determines the internalization potency of PSMA inhibitor. Therefore, many efforts have been made to improve the affinity and pharmacokinetic properties by introducing various spacers into the PSMA targeting molecule [51–53].

Considering the importance of hydrophobic motifs in a targeting molecule, we synthesized an asymmetrical glutamate-urea-lysine-based PSMA inhibitor containing an aromatic ring (Phe-Phe) in the linker (**10**) and compared it to a PSMA inhibitor containing only a straight alkyl chain (**5**). Isonitrile residues were incorporated to PSMA inhibitors **5** and **10** to obtain **15** and **16**, respectively. **15** and **16** were radiolabeled with^{99m}Tc using [^{99m}Tc][Tc$(OH_2)_3(CO)_3]^+$ in high radiochemical yield (≥98.5%). The labeled products were subsequently purified by radio-HPLC to a high radiochemical purity (≥99.5%) to remove remaining ligands and other ^{99m}Tc species (Figure 1). In order to validate the structure of [^{99m}Tc]Tc-**15** and [^{99m}Tc]Tc-**16**, macroscale reaction was carried out with cold [Re$(CO)_3(H_2O)_3]^+$ and a ^{99m}Tc analogue having similar chemistry for standard chemical characterization. HPLC profiles of Re-**15** and Re-**16** coincided well with the respective radioactive analogues [^{99m}Tc]Tc-**15** and [^{99m}Tc]Tc-**16**, suggesting that both [^{99m}Tc]Tc-**15** and [^{99m}Tc]Tc-**16** possessed the proposed trivalent structure (Figures S30 and S31).

It is very important to investigate the stability of ^{99m}Tc-labeled conjugates in view of future clinical applications. [^{99m}Tc]Tc-**15** and [^{99m}Tc]Tc-**16** demonstrate high stability in human serum up to 6 h with no sign of decomposition owing to well-known fact that isonitrile complexes are highly stable and inert under physiological conditions. Hydrophilicity is usually reported in LogD, which is an important predictor to determine the pharmacokinetics of radiopharmaceutical and is usually measured by partitioning the radiotracer between *n*-octanol and PBS buffer (pH 7.4) under strict equilibrium conditions. The low LogD value of [^{99m}Tc]Tc-**15** compared to [^{99m}Tc]Tc-**16** suggests that it is more hydrophilic. However, the presence of two phenyl amino acid groups in the spacer did not show much influence on the LogD value compared to other reports, likely because the phenyl amino groups are hindered inside the trivalent complex [4,54].

The dissociation constants (K_d) of [^{99m}Tc]Tc-**15** and [^{99m}Tc]Tc-**16** were evaluated using the 22Rv1 cell line, which has moderate PSMA expression [55,56]. [^{99m}Tc]Tc-**16** showed higher binding affinity (0.2 nM) than [^{99m}Tc]Tc-**15** (5.5 nM). Both of them were higher than the tripeptide-based monodentate ^{99m}Tc-labeled ligand (13.8 nM)[34] and comparable to MIP-1404 (1.07 nM) a highly potent PSMA targeting probe [57]. One reason for the high binding affinity may be because of the decreased dissociation rate from the cell surface due to the multimerization effect, which has been reported previously [17,58].

Tissue distribution of [^{99m}Tc]Tc-**15** and [^{99m}Tc]Tc-**16** were evaluated in 22Rv1 tumor bearing BALB/c nude mice at 1 and 4 h post-tail vein injection (Tables 1 and 2). [^{99m}Tc]Tc-**16** showed rapid accumulation at the tumor site (1 h post-injection) and the tumor uptake increased at 4 h post-injection. In contrast, [^{99m}Tc]Tc-**15** showed a moderate uptake in the tumor tissue and decreased at 4 h post-injection. The uptakes in all tumor tissues were significantly reduced by co-injection of 2-PMPA, demonstrating that the tumor uptakes are PSMA-specific for both [^{99m}Tc]Tc-**15** and [^{99m}Tc]Tc-**16**. [^{99m}Tc]Tc-**16** is rapidly cleared from blood and showed approximately 2 times higher tumor-to-blood and tumor-to-muscle ratio compared to [^{99m}Tc]Tc-**15** at 1 h post-injection, which subsequently increased to 6.4 times higher at 4 h post-injection, resulting in a high tumor-to-background ratio. Furthermore, [^{99m}Tc]Tc-**15** demonstrated high accumulation of radioactivity in kidney (~3 times higher) compared to [^{99m}Tc]Tc-**16** at 1 h post-injection. The uptakes in the kidney and spleen were inhibited by co-injection of 2-PMPA, indicating that the uptakes in these organs were mainly mediated by binding to PSMA. Similar results have been reported for other PSMA-targeting agents [59–63]. Another reason for high kidney uptake is the hydrophilic nature of [^{99m}Tc]Tc-**15** and [^{99m}Tc]Tc-**16**,which makes the kidney the primary excretion pathway. With regard to clinical translation, however, the expression of PSMA in the kidneys of nude mice is higher than expression levels in human kidneys [3,64].

The feasibility of [^{99m}Tc]Tc-**15** and [^{99m}Tc]Tc-**16** as PSMA imaging agents was tested by SPECT/CT using 22Rv1 tumor bearing BALB/c mice (Figures 3 and 4). [^{99m}Tc]Tc-**16** clearly allows for the visualization of tumor tissues after 1 h post-injection and showed prolonged retention of activity until 4 h (Figure 4). [^{99m}Tc]Tc-**16** was cleared from non-targeted tissues and showed improved images with high tumor-to-background contrast at 4 h post-injection (Figure 4). [^{99m}Tc]Tc-**15** was more rapidly excreted from the blood and showed poor tumor-to-background contrast (Figure 3). Blocking experiments by co-injection of 2-PMPA demonstrated that the tumor and kidney uptakes were specifically mediated by PSMA (Figures 3 and 4).

4. Experimental

4.1. General

All commercially available chemicals were of analytical grade and were used without further purification. Anhydrous dichloromethane (DCM), triethylamine (TEA), anhydrous methanol, triphosgene, 10% palladium on activated carbon (10% Pd/C), 9-Fluorenylmethoxycarbonyl chloride (Fmoc-Cl), *N*,*N*-diisopropylethylamine (DIPEA), *N*,*N*,*N*′,*N*′-Tetramethyl-*O*-(1*H*-benzotriazol-1-yl)uronium hexafluorophosphate (HBTU), piperidine,

N,*N*-dimethylformamide (DMF), formic acid, acetic anhydride, *N*,*N*′-dicyclohexylcarodiimide (DCC), trifluoroacetic acid (TFA), 2-(Phosphonomethyl)-pentandioic acid (2-PMPA) were purchased from Sigma-Aldrich, Korea. L-glutamic acid di-*tert*-butyl ester hydrochloride, *N*′-Cbz-L-lysine *tert*-butyl ester, 6-aminiohexanoic acid, *N*-(9-Fluorenylmethoxycarbonyl)-L-phenylalanine (Fmoc-Phe–OH), and 2,3,5,6-tetrafluorophenol (TFP) were obtained from Tokyo Chemical Industry CO., Ltd. (Tokyo, Japan). 6-(Fmoc-amino)hexanoic acid (Fmoc-6-Ahx–OH) and Boc-6-aminohexanoic acid (Boc-6-Ahx–OH) were prepared according to reported methods [65,66]. Compounds 12–14 were prepared according to reported method [47]. The 22Rv1 cell line (human prostate carcinoma epithelial cell line) was obtained from the American Type Culture Collection (ATCC). Na[$^{99m}TcO_4$] was eluted from a $^{99}Mo/^{99m}Tc$ generator using saline obtained from Unitech (Korea). The radioactive precursor [^{99m}Tc][$Tc(H_2O)_3(CO)_3$]$^+$ was prepared using an IsoLink kit (Paul Scherrer Institute, Villigen, Switzerland). Radio-thin layer chromatography (TLC) was performed with silica plates (Silica gel 60 F_{254}, Merck Ltd., Seoul, Korea) and counted using a Bio-Scan AR-2000 system scanner (Bioscan, WI, USA). Reverse phase preparative and analytical high-performance liquid chromatography (RP-HPLC) assays were performed using Xterra RP18 10 µm (10 mm × 250 mm) and Xterra RP18 3.5 µm (4.6 mm × 100 mm) columns (Waters Co. Milford, MA, USA), respectively. Sep-Pak C18 cartridges (130 mg, 55–105 µm) were obtained from Waters, Dublin, Ireland. Mass spectra (ESI/MS) were recorded on a Thermofisher LTQ Velos instrument in positive ionization mode. Matrix-assisted laser desorption ionization time-of-flight (MALDI-TOF) was performed using Voyager DE-STR (Applied Biosystems, Seoul, Korea). H NMR spectra were recorded on an Avance-500 NMR spectrometer (500 MHz for H; Bruker, Seongnam, Korea) and an AL-300 FT NMR spectrometer (300 MHz for H; Jeol, Tokyo, Japan). The chemical shifts are reported in parts per million (ppm). The following abbreviations are used for the description of H NMR spectra: singlet (s), doublet (d), triplet (t), quartet (q), multiplet (m), doublet of doublets (dd), triplet of doublet (td), doublet of triplet (dt), triplet of triplet (tt), doublet of quartets (dq), doublet of doublet of double (ddd), triplet of double of doublet (tdd), doublet of triplet of triplet (dtt). Micro-SPECT/CT imaging studies were performed on a nanoSPECT/CT plus device (Mediso, Budapest, Hungary).

4.2. Cell Culture and Tumor Model

22Rv1 cells were cultured as monolayers in RPMI-1640 medium at 37 °C in a humidified atmosphere containing 5% CO_2. RPMI was supplemented with 10% fetal bovine serum, 4.5 g/L D-glucose, 2 mM L-glutamine, 1 mM sodium pyruvate, and 1.5 g/L sodium bicarbonate. 22Rv1 tumor xenografts were established with male BALB/c nude mice (3–4 weeks old). Briefly, approximately, 5×10^6 cultured 22Rv1 cells were suspended in RPMI-640 media and subcutaneously implanted (100 µL) into the upper right flank of mice. Ex vivo biodistribution and imaging studies were performed once the tumor reached 100–400 mm^3 in volume (3–4 weeks). All animal experiments (#3520150085, approval date 9 November 2015) were performed in compliance with the Seoul National University Hospital, Seoul, Korea, which is accredited by the Association for Assessment and Accreditation of Laboratory Animal Care (AAALAC International, 2007).

4.3. Chemical Synthesis

Tri-*tert*-butyl (13S)-3,11-dioxo-1-phenyl-2-oxa-4,10,12-triazapentadecane-9,13,15-tricarboxylate (1). A solution of L-glutamic acid di-*tert*-butyl ester hydrochloride (2.3 g, 7.88 mmol) in anhydrous DCM (60 mL) was added to TEA (2.6 mL, 25.7 mmol) at −78 °C and stirred for 30 min under a nitrogen atmosphere. Triphosgene (0.8 g, 2.6 mmol) was added dropwise over a period of 1 h and stirred at room temperature (rt) for 1 h followed by addition of *N*′-Cbz-L-lysine *tert*-butyl ester (1.6 g, 4.7 mmol) containing TEA (0.4 mL, 4.7 mmol) in DCM (20 mL) in one portion. The mixture was allowed to react overnight (18 h). After the completion of the reaction, the organic layer was washed with a saturated solution of $NaHCO_3$ (1 × 50 mL), water (2 × 50 mL), and finally with brine (1 × 30 mL). The organic layer was separated and dried over anhydrous sodium sulfate, concentrated under reduce

pressure, and purified by silica gel column chromatography using DCM and Methanol (95:5, *v*/*v*) to yield colorless oil (1.9 g, 66%). ^{1}H NMR (500 MHz, $CDCl_3$) δ 7.37–7.27 (m, 5H), 5.13–5.07 (m, 2H), 4.32 (td, J = 8.4, 4.8 Hz, 2H), 3.23–3.10 (m, 2H), 2.33–2.23 (m, 2H), 1.90–1.70 (m, 2H), 1.66–1.46 (m, 4H), 1.46–1.26 (m, 31H). ESI-MS, (*m*/*z*): $[M + H]^+$, 622.

Di-*tert*-butyl ((6-amino-1-(*tert*-butoxy)-1-oxohexan-2-yl)carbamoyl)-L-glutamate (2). 10% Pd/C (100 mg) was added to the solution described above in **1** (1.5 g, 2.4 mmol) in methanol (20 mL). The suspension was stirred for 18 h under a hydrogen atmosphere. After the completion of the reaction, Pd/C was removed by passing it though Celite®. The filtrate obtained was concentrated under reduced pressure to obtained colorless oil (quantitative yield), which solidified on standing over a period of time. We then proceeded to the next step without further purification. ^{1}H NMR (500 MHz, $CDCl_3$) δ 4.31–4.22 (m, 2H), 2.34–2.30 (m, 2H), 1.89–1.77 (m, 2H), 1.77–1.62 (m, 4H), 1.58–1.47 (m, 2H), 1.46–1.28 (m, 29H). ESI-MS, (*m*/*z*): $[M + H]^+$, 488.

Tri-*tert*-butyl (20S)-1-(9H-fluoren-9-yl)-3,10,18-trioxo-2-oxa-4,11,17,19-tetraazadocosane-16,20,22-tricarboxylate (3). Fmoc-6-Ahx–OH (505 mg, 1.43 mmol) in DMF (15 mL) and DIPEA (1 mL, 3.5 mmol) were added to the solution obtained in **2** (500 mg, 1.0 mmol), and stirred at 0 °C for 10 min under an inert atmosphere. HBTU (585 mg, 1.5 mmol) in DMF (5 mL) was added dropwise and the reaction mixture was stirred for 18 h at RT. After the completion of the reaction, ethyl acetate (50 mL) was added and the organic layer was washed with water (3 × 30 mL), dried over Na_2SO_4, and concentrated under reduce pressure. The crude product obtained was purified by silica gel column chromatography using DCM/methanol (97: 3, *v*/*v*) to produce a white solid product (494 mg, 60%). ^{1}H NMR (500 MHz, $CDCl_3$) δ 7.78–7.74 (m, 2H), 7.60 (d, *J* = 7.4 Hz, 2H), 7.42–7.37 (m, 2H), 7.31 (td, *J* = 7.5, 1.2 Hz, 2H), 4.39 (dt, *J* = 10.1, 5.2 Hz, 2H), 4.36–4.26 (m, 2H), 4.25–4.18 (m, 1H), 3.38–3.06 (m, 4H), 2.32 (tdd, *J* = 13.4, 9.3, 6.3 Hz, 2H), 2.19 (dd, *J* = 13.8, 6.6 Hz, 2H), 2.11–2.03 (m, 2H), 1.88–1.75 (m, 2H), 1.58–1.33 (m, 37H). ESI-MS, (*m*/*z*): $[M + H]^+$, 823.

Di-*tert*-butyl ((6-(6-aminohexanamido)-1-(*tert*-butoxy)-1-oxohexan-2-yl)carbamoyl)-L-glutamate (4). The solution described in **3** (500 mg, 0.6 mmol) was dissolved in 20% piperidine/DMF (1 mL) and was stirred at RT for 1 h. The solvent was removed under vacuum and the product was purified by HPLC (method **1**) to yield a white solid product (306 mg, 80%). ^{1}H NMR (500 MHz, $CDCl_3$) δ 4.18 (p, *J* = 5.0 Hz, 2H), 2.32 (t, *J* = 7.5 Hz, 2H), 2.28–2.22 (m, 2H), 2.09–1.85 (m, 2H), 1.69 (ddd, *J* = 24.0, 18.3, 11.1 Hz, 6H), 1.58–1.23 (m, 37H). ESI-MS, (*m*/*z*): $[M + H]^+$, 601.

((5-(6-Aminohexanamido)-1-carboxypentyl)carbamoyl)-L-glutamic acid (5). The product obtained in **4** (200 mg, 0.33 mmol) was dissolved in a mixture of TFA and DCM (2 mL, 1: 1 *v*/*v*) and was stirred overnight at RT. After completion of the reaction, the solvent was removed by reduced pressure and the residue was purified by HPLC (method **2**) to obtain a white solid product (56, 39%). ^{1}H NMR (500 MHz, Methanol-d_4) δ 4.27 (ddd, *J* = 31.1, 8.6, 5.0 Hz, 2H), 3.17 (t, *J* = 6.8 Hz, 2H), 2.91 (t, *J* = 7.6 Hz, 2H), 2.40 (ddd, *J* = 8.5, 6.8, 4.2 Hz, 2H), 2.20 (t, *J* = 7.3 Hz, 2H), 1.71–1.60 (m, 10H), 1.45–1.35 (m, 4H). (ESI-MS, (*m*/*z*): $[M + H]^+$, 433.

Tri-*tert*-butyl (23S)-5-benzyl-1-(9H-fluoren-9-yl)-3,6,13,21-tetraoxo-2-oxa-4,7,14,20,22-pentaazapentacosane-19,23,25-tricarboxylate (6). A solution of **4** (800 mg, 1.33 mmol), Fmoc–Phe–OH (515 mg, 1.33), and DIPEA (0.8 mL, 4.65 mmol) in DMF (6 mL) was cooled to 0 °C and stirred for 10 min. HBTU (1.0 g, 2.7 mmol) in DMF (2 mL) was added dropwise and the reaction mixture was allowed to stir at RT for 18 h. After the completion of the reaction, ethyl acetate (20 mL) was added and the organic layer was washed with water (3 × 40 mL), dried over Na_2SO_4, and concentrated under reduce pressure. The product obtained was purified by silica gel column chromatography using DCM and methanol (96: 4, *v*/*v*) to produce a white solid (839 mg, 65%). ^{1}H NMR (500 MHz, $CDCl_3$) δ 7.75 (dt, *J* = 7.6, 0.9 Hz, 2H), 7.39 (t, *J* = 7.4 Hz, 2H), 7.30–7.20 (m, 9H), 4.52–4.34 (m, 4H), 4.30 (t, *J* = 9.1 Hz, 1H), 4.18 (t, *J* = 7.1 Hz, 1H), 3.17 (d, *J* = 6.4 Hz, 2H), 3.06 (d, *J* = 7.2 Hz, 2H), 2.37–2.27 (m, 2H), 2.26–2.01 (m, 4H), 1.89–1.74 (m, 2H), 1.68–1.56 (m, 2H), 1.55–1.22 (m, 37H). ESI-MS, (*m*/*z*): $[M + H]^+$, 971.

Tri-*tert*-butyl (3S)-21-amino-5,13,20-trioxo-22-phenyl-4,6,12,19-tetraazadocosane-1,3,7-tricarboxylate (7). The solution obtained in **6** (300 mg, 0.3 mmol) was dissolved in 20% piperidine/DMF (1 mL) and was allowed to stirred for 1 h at RT. The solvent was removed by vacuum and purified by HPLC (method **3**) to afford white solid (179 mg, 80%). ^{1}H NMR (500 MHz, $CDCl_3$) δ 7.28 (d, *J* = 1.8 Hz, 1H), 7.26–7.20 (m, 4H), 4.33 (t, *J* = 7.3 Hz, 1H), 4.24 (dt, *J* = 8.7, 5.3 Hz, 2H), 3.35–3.08 (m, 6H), 2.31 (td, *J* = 7.4, 6.6, 1.7 Hz, 2H), 2.16 (t, *J* = 6.9 Hz, 2H), 1.66–1.50 (m, 4H), 1.49–1.28 (m, 37H). ESI-MS, (*m*/*z*): $[M + H]^+$, 748.

Tri-*tert*-butyl (8R,26S)-5,8-dibenzyl-1-(9H-fluoren-9-yl)-3,6,9,16,24-pentaoxo-2-oxa-4,7,10,17,23,25-hexaazaoctacosane-22,26,28-tricarboxylate (8). The product **7** (526 mg, 0.7 mmol), was dissolved in a mixture of Fmoc–Phe–OH (299 mg, 0.7 mmol) and DIPEA (0.43 mL, 4.65 mmol) in DMF (3 mL) and was cooled to 0 °C and stirred for 10 min. HBTU (530 mg, 1.4 mmol) in DMF (2 mL) was added dropwise over a period of 10 min. After stirring the reaction mixture for 18 h at RT, ethyl acetate (30 mL) was added and the organic layer washed with water (3 × 40 mL), dried over Na_2SO_4, and concentrated under reduce pressure. The product was purified by silica gel column chromatography using DCM and methanol (96: 3,) to yield a white solid product (531 mg, 68%). ^{1}H NMR (500 MHz, $CDCl_3$) δ 7.51–7.46 (m, 2H), 7.39 *v*/*v* (t, *J* = 7.4 Hz, 2H), 7.30–7.11 (m, 14H), 4.68 (d, *J* = 7.7 Hz, 1H), 4.51–4.29 (m, 4H), 4.21 (t, *J* = 8.9 Hz, 1H), 4.14 (t, *J* = 7.2 Hz, 1H), 3.29–2.80 (m, 8H), 2.37–2.21 (m, 4H), 2.10–2.01 (m, 2H), 1.89–1.74 (m, 2H), 1.62–1.26 (m, 37H). ESI-MS, (*m*/*z*): $[M + H]^+$, 1118.

Tri-*tert*-butyl (3S,21R)-24-amino-21-benzyl-5,13,20,23-tetraoxo-25-phenyl-4,6,12,19,22-pentaazapentacosane-1,3,7-tricarboxylate (9). The product **8** (300 mg, 0.3 mmol) was dissolved in 20% piperidine/DMF solution (1 mL) was stirred at RT for 1 h. The solvent was removed by under vacuum and the product was purified by HPLC (method **4**) to afford white solid (215 mg, 90%). ^{1}H NMR (500 MHz, $CDCl_3$) δ 7.25–7.09 (m, 10H), 4.58 (q, *J* = 7.6 Hz, 1H), 4.30 (d, *J* = 10.3 Hz, 2H), 3.30 (dd, *J* = 13.5, 6.9 Hz, 1H), 3.21–3.00 (m, 6H), 2.93–2.83 (m, 1H), 2.36–2.22 (m, 2H), 2.10 (dtt, *J* = 35.8, 14.2, 7.6 Hz, 4H), 1.86–1.67 (m, 2H), 1.49–1.14 (m, 37H). ESI-MS, (*m*/*z*): $[M + H]^+$, 896.

Tri-*tert*-butyl (16R,34S)-13,16-dibenzyl-2,2-dimethyl-4,11,14,17,24,32-hexaoxo-3-oxa-5,12,15,18,25,31,33-heptaazahexatriacontane-30,34,36-tricarboxylate (10). The solution obtained in **9** (150 mg, 0.2 mmol) was mixed with Boc-6-Ahx–OH (42 mg, 0.2 mmol) and DIPEA (0.1 mL, 0.6 mmol) and dissolved in in DMF (2 mL),then cooled to 0 °C. HBTU (127 mg, 1.4 mmol) in DMF (1mL) was added dropwise. After stirring the reaction mixture at RT for 18 h, ethyl acetate (15 mL) was added and the organic layer washed with water (3 × 20 mL), dried over Na_2SO_4, and concentrated under reduce pressure. The mixture was purified by silica gel column chromatography using DCM and MeOH (96:3, *v*/*v*) to yield a white solid product (155 mg, 70%). ^{1}H NMR (500 MHz, $CDCl_3$) δ 7.26–7.10 (m, 10H), 4.74–4.58 (m, 3H), 4.45 (q, *J* = 6.5 Hz, 2H), 3.25–2.82 (m, 9H), 2.39–2.15 (m, 5H), 2.09 (dt, *J* = 13.0, 6.5 Hz, 4H), 1.92–1.71 (m, 2H), 1.68–1.30 (m, 52H). ESI-MS, (*m*/*z*): $[M + H]^+$, 1109.

(3S,21R)-31-amino-21,24-dibenzyl-5,13,20,23,26-pentaoxo-4,6,12,19,22,25-hexaazahentriacontane-1,3,7-tricarboxylic acid (11). The solution produced in **10** (50 mg, 0.05) was dissolved in a mixture of TFA and DCM (2 mL, 1: 1, *v*/*v*) and was stirred overnight at RT. After completion of the reaction, the solvent was removed by reduced pressure and the residue was purified by HPLC (method 4) to yield a white solid product (17 mg, 44%). ^{1}H NMR (500 MHz, Methanol-d4) δ 7.34–7.11 (m, 10H), 4.69–4.47 (m, 2H), 4.30 (ddd, *J* = 14.8, 8.4, 4.9 Hz, 2H), 3.21–3.13 (m, 2H), 3.08 (ddt, *J* = 13.4, 6.8, 2.9 Hz, 4H), 2.99–2.74 (m, 4H), 2.41 (ddd, *J* = 8.2, 6.9, 1.9 Hz, 2H), 2.21–2.08 (m, 4H), 1.96–1.77 (m, 2H), 1.61 (s, 2H), 1.58–1.12 (m, 16H). ESI-MS, (*m*/*z*): $[M + H]^+$, 841.

(3S)-22-isocyano-5,13,20-trioxo-4,6,12,19-tetraazadocosane-1,3,7-tricarboxylic acid (15). A solution of the product of **5** (90 mg, 0.2 mmol) and DIPEA (2.5 eq) in anhydrous methanol (2 mL) was and stirred for 10 min at RT. The product of **14** (77 mg, 0.3 mmol) was dissolved in anhydrous methanol (1 mL) and was added dropwise and stirred under a nitrogen atmosphere for 5 h. The solvent was removed using a rotary evaporator and the product was purified by RP-HPLC (method **5**) and lyophilized to obtain

oily compound (35 mg, 34%). 1H NMR (500 MHz, Methanol-d4) δ 4.23 (ddd, *J* = 18.8, 8.6, 4.9 Hz, 2H), 3.13 (t, *J* = 6.7 Hz, 2H), 2.87 (t, *J* = 7.7 Hz, 2H), 2.40–2.31 (m, 2H), 2.16 (t, *J* = 7.3 Hz, 2H), 1.90–1.72 (m, 2H), 1.66–1.27 (m, 14H). ESI-MS, (*m/z*): $[M + H]^+$, 514.

(3S,21R)-21,24-dibenzyl-35-isocyano-5,13,20,23,26,33-hexaoxo-4,6,12,19,22,25,32-heptaazapentatriacontane-1,3,7-tricarboxylic acid (16). DIPEA (2.5 eq) was added to a solution of the product of **11** (35 mg, 0.039 mmol) in anhydrous methanol (1 mL) and stirred at RT for 10 min. A solution of the product of **14** (14 mg, 0.05 mmol) in methanol (1 mL) was added and stirred for 5 h. After completion of the reaction, the solvent was removed using a rotary evaporator and purified by HPLC (method **6**) to yield a white solid product (14 mg, 40%). 1H NMR (500 MHz, Methanol-d4) δ 7.22 (dq, *J* = 14.6, 7.0 Hz, 10H), 4.56 (ddd, *J* = 14.1, 8.9, 6.0 Hz, 2H), 4.24 (td, *J* = 7.7, 4.8 Hz, 2H), 3.25–2.88 (m, 12H), 2.54 (s, 2H), 2.38 (ddd, *J* = 8.7, 6.6, 2.7 Hz, 2H), 2.17–2.06 (m, 4H), 1.59 (ddd, *J* = 30.6, 14.5, 7.2 Hz, 4H), 1.46–1.14 (m, 16H). ESI-MS, (*m/z*): $[M + H]^+$, 921.

Re-15 and Re-16. The cold rhenium precursor $[Re(CO)_3(H_2O)_3]Br$ was synthesized according to a reported method [67]. In brief, bromopentacarbonylrhenium(I) (100 mg, 0.25 mmol) was refluxed for 24 h in deionized water (5 mL) to obtain $[Re(CO)_3(H_2O)_3]Br$ at a final concentration of 2 mg/mL. For synthesis of Re-**15**, $[Re(CO)_3(H_2O)_3]Br$ (400 µL, 1 µmol) was added to a solution of precursor **15** (11 mg, 0.02 mmol) in methanol (2 mL) and heated at 100 °C for 4 h. For Re-**16**, $[Re(CO)_3(H_2O)_3]Br$ (400 µL, 1 µmol) was added to a solution of **16** (10 mg, 0.01 mmol) in a mixture of methanol and water (3 mL, 1:1 *v/v*). The reaction mixture was heated for 3 h at 100 °C. The resulting mixture was concentrated in a rotary evaporator and injected in to a HPLC (method **7** or **8**).

4.4. Radiolabeling of [^{99m}Tc]Tc-15 and [^{99m}Tc]Tc-16

$[^{99m}Tc][Tc(H_2O)_3(CO)_3]$ precursor was prepared using an IsoLink kit. A kit containing sodium tetraborate decahydrate (2.9 mg), sodium carbonate (7.8 mg), potassium sodium tartrate tetrahydrate (9.0 mg), and disodium boranocarbonate (4.5 mg) was added $[^{99m}TcO_4]^-$(1 mL, 555–740 MBq). The vial was heated on a heating block for 30 min at 100 °C and equilibrated at RT for 10 min. The pH (6–6.5) was adjusted by addition of 1 N HCl (200 µL). The radiochemical purity was determined by radio-HPLC (method **7** or **8**). A freshly prepared solution of $[^{99m}Tc][Tc(H_2O)_3(CO)_3]^+$ (500 µL, 370 MBq) was added to a vial containing **15** or **16** in a mixture of methanol and water (100 µg, 200 µL, 3:1 *v/v*). The vial was heated for 30 min at 100 °C, followed by purification by radio-HPLC (method **7** or **8**). The eluted fractions containing ^{99m}Tc-labeled conjugates were collected and diluted with water (20 mL) and passed through a Sep-Pak C18 cartridge, which was preconditioned with ethanol (12 mL) and water (12 mL). After washing the Sep-Pak C18 cartridge with water (5 mL), the ^{99m}Tc-labeled conjugates were eluted with ethanol (1 mL) and diluted with saline for further in vitro and imaging studies.

4.5. In Vitro Stability Tests in Serum

In vitro stability of the ^{99m}Tc labeled conjugates were tested in human serum. In brief, [^{99m}Tc]Tc-**15** or **16** (25.9 MBq, 200 µL) was incubated with human serum (500 µL) in an incubator at 37 °C with gentle shaking. After 1, 3, and 6 h, an aliquot of the solution (50 µL) was added to methanol (100 µL). The resulting supernatant was centrifuged and radiochemical purity was determined by radio-TLC and radio-HPLC.

4.6. Determination of Distribution Coefficient (LogD Value)

The distribution coefficients (LogD values) of the ^{99m}Tc labeled conjugates were determined by measuring the activity that partitioned between 1-octanol and PBS (50 mM, pH 7.4) under equilibrium conditions. Briefly, [^{99m}Tc]Tc-**15** or [^{99m}Tc]Tc-**16** purified by radio-HPLC and solvent was removed by rotary evaporator. The residue obtained was dissolved in 3 mL PBS (50 mM, pH 7.4) to a concentration of 2.5 MBq/mL in triplicate. Anhydrous 1-octanol was added (3 mL) and the mixture was vortexed for 5 min and centrifuged at 3300 r/min for 5 min to separate the layers. The counts in the organic

and inorganic layers (100 µL) were determined using an γ-counter (Cobra II automated γ-counter). The LogD was calculated using the following equation: LogD = Log(cpm in octanol − cpm in background)/(cpm in buffer − cpm in background).

4.7. Measurement of Binding Affinity (K_d) In Vitro

To evaluate the binding affinity of [^{99m}Tc]Tc-**15** and [^{99m}Tc]Tc-**16**, K_d was investigated using a saturation binding assay. 22Rv1 cells (1×10^5 cells/well, 1 mL) were plated into a 24-well flat-bottom plate and allowed to form an adherent monolayer. The medium in each well was then replaced with HBSS supplemented with 1% bovine serum albumin, containing increasing concentrations of [^{99m}Tc]Tc-**15** or [^{99m}Tc]Tc-**16** in serial dilutions. The cells were incubated for 1 h at 37 °C with shaking. After 1 h, the media was aspirated and the cells were washed with HBSS (3 mL × 2) to remove unbound activity. Cells were lysed by adding sodium dodecyl sulfate (0.5% in PBS, 500 µL) to each well and mixed to dissolve the cells, and the lysates were transferred to plastic tubes (4 mL). The radioactivity of each sample was counted using a γ-counter (Cobra II automated γ-counter), along with reference samples which contained the total amount of added radioactivity. Nonspecific binding was determined in the presence of 2-PMPA (250 µM). Specific binding was calculated by subtracting the nonspecific bound radioactivity from that of the total binding. The K_d was calculated by non-linear regression using GraphPad Prism 7 (GraphPad Software Inc., San Diego, CA, USA) using a one site binding equation.

4.8. Ex Vivo Biodistribution Study

The ex vivo biodistribution of [^{99m}Tc]Tc-**15** or [^{99m}Tc]Tc-**16** was evaluated in 22Rv1 tumor-bearing male nude mice (22–25 g). [^{99m}Tc]Tc-**15** or [^{99m}Tc]Tc-**16** (74 kBq, 100 µL) was administered via a lateral tail vein in each mice. The mice were sacrificed at 1 and 4 h post-injection. The relevant tissues and organs were excised and collected. The collected tissues and organs were washed with saline, dried, weighed, and counted using an automatic γ-counter. In order to confirm the specific uptake, mice were co-injected with 2-PMPA (100 µg). Uptake in each tissues and organ was expressed as the percentage of the injected dose per gram (% ID/g). A standard solution was additionally prepared to estimate the total dose injected per mice. Values are expressed as the mean ± standard deviation (SD).

4.9. SPECT/CT Imaging

The SPECT/CT images were taken at 1 and 3 h for [^{99m}Tc]Tc-**15** (7.4MBq/200 µL) and for [^{99m}Tc]Tc-**16** (7–6 MBq/200 µL) images were acquired at 1 and 4 h after the administration of ^{99m}Tc-labeled conjugates to 22Rv1 tumor-bearing BALB/c male nude mice through the tail vein. For blockade experiment, mice were co-injected with potent inhibitor 2-PMPA (100 µg) to confirm uptake in the tumor was PSMA mediated. For SPECT/CT imaging, mice were anesthetized with isoflurane and scanned with a nanoScan SPECT/CT device. The scanning acquisition parameters for imaging modality are 140 keV ± 10% γ-ray energy window, 256 × 256 matrix size, 5 Section per angular step of 18° of time acquisition, and a reconstruction algorithm of ordered subset expectation maximization with nine iterations. For CT, a tube voltage of 45 kVp, an exposure time of 1.5 Section per projection, and a reconstruction algorithm of cone-beam filtered back-projection was used. Images were processed using Invivoscope processing software. A Gauss reconstruction filter was used to the SPECT images and scale is adjusted to allow visualization of organs and tissues of interest.

Statistical Analysis. Statistical analyses were performed by Student's *t*-test. The difference was considered statistically significant when the p values were ≤ 0.05.

5. Conclusions

We successfully synthesized [^{99m}Tc]Tc-**15** and [^{99m}Tc]Tc-**16** for imaging PSMA and evaluated their binding affinities in vitro and targeting capabilities in vivo. The in vitro study results demonstrated that [^{99m}Tc]Tc-**16** has a higher binding affinity compared to [^{99m}Tc]Tc-**15**, possibly because of its interaction with the S1 hydrophobic pocket and multimeric effects. Ex vivo biodistribution study for

both ^{99m}Tc-labeled conjugates demonstrated significantly improved tumor uptake and retention of [^{99m}Tc]Tc-**16** compared to [^{99m}Tc]Tc-**15** up to 4 h post-injection. The tumor uptakes were blocked by co-injection of 2-PMPA, suggesting that the uptake is PSMA mediated. Finally, whole-body SPECT/CT image demonstrated the feasibility of [^{99m}Tc]Tc-**16** as an efficient imaging agent for PSMA-expressing tumors with higher tumor-to-background ratio compared to [^{99m}Tc]Tc-**15**.

Supplementary Materials: The following are available online at http://www.mdpi.com/2304-6740/8/1/5/s1, Figure S1: HPLC profiles of hot and cold complexes, Figure S2: Saturation binding curve (A) [^{99m}Tc]Tc-**15** (B) [^{99m}Tc]Tc-**16**, Figure S3: ^{1}H-NMR of **2**, Figure S4: ESI-MS spectrum of **2,** Figure S5: ^{1}H-NMR of **3,** Figure S6: ESI-MS spectrum of **3,** Figure S7: ^{1}H-NMR of **4**, Figure S8: ESI-MS spectrum of **4**, Figure S9: ^{1}H-NMR of **5,** Figure S10: ESI-MS spectrum of **5,** Figure S11: ^{1}H-NMR of **6,** Figure S12: ESI-MS spectrum of **6,** Figure S13: ^{1}H-NMR of **7**, Figure S14: ESI-MS spectrum of **7,** Figure S15: ^{1}H-NMR of **8,** Figure S16: ESI-MS spectrum of **8,** Figure S17: ^{1}H-NMR of **9,** Figure S18: ESI-MS spectrum of **9,** Figure S19: ^{1}H-NMR of **10**, Figure S20: ESI-MS spectrum of **10**, Figure S21: ^{1}H-NMR of **11**, Figure S22: ESI-MS spectrum of **11**, Figure S23: ^{1}H-NMR compound **12**, Figure S24: ^{1}H-NMR of compound **13**, Figure S25: ^{1}H-NMR of compound **14**, Figure S26: ^{1}H-NMR of compound **15**, Figure S27: ESI-MS spectrum of **15**, Figure S28: ^{1}H-NMR of **16**, Figure S29: ESI-MS spectrum of **16**, Figure S30: ESI-MS spectrum of Re-**15**, Figure S31: MALDI-TOF spectrum of Re-**16**.

Author Contributions: Original writing-first draft, N.A.L.; performed experiment, N.A.L., J.Y.P., K.K., M.K.H., Y.J.K.; conceptualization, Y.-S.L.; review and editing, Y.-S.L., G.J.C., K.W.K.; supervision, J.M.J. All authors have read and agreed to the published version of the manuscript.

Funding: This work was supported by the Technology Innovation Program (20001235, Development of Novel Radiopharmaceutical for Prostate Cancer Targeted Imagining Diagnosis) funded by the Ministry of Trade, Industry & Energy (MOTIE, Korea. This research was also supported by the Ministry of Health and Welfare (Grant Number: HI15C3093). This research was also supported by National Research Foundation (2017M2A2A7A01071134).

Conflicts of Interest: The authors declare that they have no conflicts of interest.

References

1. Siegel, R.L.; Miller, K.D.; Jemal, A. Cancer statistics, 2018. CA. *Cancer J. Clin.* **2018**, *68*, 7–30. [CrossRef]
2. Bouchelouche, K.; Choyke, P.L.; Capala, J. Prostate specific membrane antigen- a target for imaging and therapy with radionuclides. *Discov. Med.* **2010**, *9*, 55–61. [PubMed]
3. Ghosh, A.; Heston, W.D. Tumor target prostate specific membrane antigen (PSMA) and its regulation in prostate cancer. *J. Cell. Biochem.* **2004**, *91*, 528–539. [CrossRef] [PubMed]
4. Xu, X.; Zhang, J.; Hu, S.; He, S.; Bao, X.; Ma, G.; Luo, J.; Cheng, J.; Zhang, Y. ^{99m}Tc-labeling and evaluation of a HYNIC modified small-molecular inhibitor of prostate-specific membrane antigen. *Nucl. Med. Biol.* **2017**, *48*, 69–75. [CrossRef] [PubMed]
5. Perner, S.; Hofer, M.D.; Kim, R.; Shah, R.B.; Li, H.; Möller, P.; Hautmann, R.E.; Gschwend, J.E.; Kuefer, R.; Rubin, M.A. Prostate-specific membrane antigen expression as a predictor of prostate cancer progression. *Hum. Pathol.* **2007**, *38*, 696–701. [CrossRef] [PubMed]
6. Bravaccini, S.; Puccetti, M.; Bocchini, M.; Ravaioli, S.; Celli, M.; Scarpi, E.; De Giorgi, U.; Tumedei, M.M.; Raulli, G.; Cardinale, L.; et al. PSMA expression: A potential ally for the pathologist in prostate cancer diagnosis. *Sci. Rep.* **2018**, *8*, 4254. [CrossRef]
7. Wynant, G.E.; Murphy, G.P.; Horoszewicz, J.S.; Neal, C.E.; Collier, B.D.; Mitchell, E.; Purnell, G.; Tyson, I.; Heal, A.; Abdel-Nabi, H.; et al. Immunoscintigraphy of prostatic cancer: Preliminary results with ^{111}In-labeled monoclonal antibody 7E11-C5.3 (CYT-356). *Prostate* **1991**, *18*, 229–241. [CrossRef]
8. Silver, D.A.; Pellicer, I.; Fair, W.R.; Heston, W.D.; Cordon-Cardo, C. Prostate-specific membrane antigen expression in normal and malignant human tissues. *Clin. Cancer Res.* **1997**, *3*, 81–85.
9. Kahn, D.; Williams, R.D.; Manyak, M.J.; Haseman, M.K.; Seldin, D.W.; Libertino, J.A.; Maguire, R.T. Indium-Capromab Pendetide In the Evaluation of Patients with Residual or Recurrent Prostate Cancer After Radical Prostatectomy. *J. Urol.* **1998**, *159*, 2041–2047. [CrossRef]
10. Nagda, S.N.; Mohideen, N.; Lo, S.S.; Khan, U.; Dillehay, G.; Wagner, R.; Campbell, S.; Flanigan, R. Long-term follow-up of ^{111}In-capromab pendetide (ProstaScint) scan as pretreatment assessment in patients who undergo salvage radiotherapy for rising prostate-specific antigen after radical prostatectomy for prostate cancer. *Int. J. Radiat. Oncol. Biol. Phys.* **2007**, *67*, 834–840. [CrossRef]

11. Troyer, J.K.; Feng, Q.; Beckett, M.L.; Wright, G.L.J. Biochemical characterization and mapping of the 7E11-C5.3 epitope of the prostate-specific membrane antigen. *Urol. Oncol.* **1995**, *1*, 29–37. [CrossRef]
12. Troyer, J.K.; Beckett, M.L.; Wright, G.L.J. Location of prostate-specific membrane antigen in the LNCaP prostate carcinoma cell line. *Prostate* **1997**, *30*, 232–242. [CrossRef]
13. Bander, N.H.; Trabulsi, E.J.; Kostakoglu, L.; Yao, D.; Vallabhajosula, S.; Smith-Jones, P.; Joyce, M.A.; Milowsky, M.; Nanus, D.M.; Goldsmith, S.J. Targeting Metastatic Prostate Cancer with Radiolabeled Monoclonal Antibody J591 to the Extracellular Domain of Prostate Specific Membrane Antigen. *J. Urol.* **2003**, *170*, 1717–1721. [CrossRef] [PubMed]
14. Morris, M.J.; Divgi, C.R.; Pandit-Taskar, N.; Batraki, M.; Warren, N.; Nacca, A.; Smith-Jones, P.; Schwartz, L.; Kelly, W.K.; Slovin, S.; et al. Pilot Trial of Unlabeled and Indium-111–Labeled Anti–Prostate-Specific Membrane Antigen Antibody J591 for Castrate Metastatic Prostate Cancer. *Clin. Cancer Res.* **2005**, *11*, 7454–7461. [CrossRef] [PubMed]
15. Bander, N.H.; Milowsky, M.I.; Nanus, D.M.; Kostakoglu, L.; Vallabhajosula, S.; Goldsmith, S.J. Phase I Trial of 177Lutetium-Labeled J591, a Monoclonal Antibody to Prostate-Specific Membrane Antigen, in Patients With Androgen-Independent Prostate Cancer. *J. Clin. Oncol.* **2005**, *23*, 4591–4601. [CrossRef]
16. Pandit-Taskar, N.; O'Donoghue, J.A.; Morris, M.J.; Wills, E.A.; Schwartz, L.H.; Gonen, M.; Scher, H.I.; Larson, S.M.; Divgi, C.R. Antibody mass escalation study in patients with castration-resistant prostate cancer using ^{111}In-J591: Lesion detectability and dosimetric projections for 90Y radioimmunotherapy. *J. Nucl. Med. Off. Publ. Soc. Nucl. Med.* **2008**, *49*, 1066–1074. [CrossRef]
17. Schäfer, M.; Bauder-Wüst, U.; Leotta, K.; Zoller, F.; Mier, W.; Haberkorn, U.; Eisenhut, M.; Eder, M. A dimerized urea-based inhibitor of the prostate-specific membrane antigen for (68)Ga-PET imaging of prostate cancer. *EJNMMI Res.* **2012**, *2*, 23. [CrossRef]
18. Banerjee, S.R.; Foss, C.A.; Castanares, M.; Mease, R.C.; Byun, Y.; Fox, J.J.; Hilton, J.; Lupold, S.E.; Kozikowski, A.P.; Pomper, M.G. Synthesis and Evaluation of Technetium-99m- and Rhenium-Labeled Inhibitors of the Prostate-Specific Membrane Antigen (PSMA). *J. Med. Chem.* **2008**, *51*, 4504–4517. [CrossRef]
19. Chen, Y.; Foss, C.A.; Byun, Y.; Nimmagadda, S.; Pullambhatla, M.; Fox, J.J.; Castanares, M.; Lupold, S.E.; Babich, J.W.; Mease, R.C.; et al. Radiohalogenated Prostate-Specific Membrane Antigen (PSMA)-Based Ureas as Imaging Agents for Prostate Cancer. *J. Med. Chem.* **2008**, *51*, 7933–7943. [CrossRef]
20. Hillier, S.M.; Maresca, K.P.; Femia, F.J.; Marquis, J.C.; Foss, C.A.; Nguyen, N.; Zimmerman, C.N.; Barrett, J.A.; Eckelman, W.C.; Pomper, M.G.; et al. Preclinical Evaluation of Novel Glutamate-Urea-Lysine Analogues That Target Prostate-Specific Membrane Antigen as Molecular Imaging Pharmaceuticals for Prostate Cancer. *Cancer Res.* **2009**, *69*, 6932–6940. [CrossRef]
21. Schottelius, M.; Wirtz, M.; Eiber, M.; Maurer, T.; Wester, H.-J. PSMA-I&T: Expanding the spectrum of PSMA-I&T applications towards SPECT and radioguided surgery. *EJNMMI Res.* **2015**, *5*, 68. [CrossRef] [PubMed]
22. Maresca, K.P.; Marquis, J.C.; Hillier, S.M.; Lu, G.; Femia, F.J.; Zimmerman, C.N.; Eckelman, W.C.; Joyal, J.L.; Babich, J.W. Novel Polar Single Amino Acid Chelates for Technetium-99m Tricarbonyl-Based Radiopharmaceuticals with Enhanced Renal Clearance: Application to Octreotide. *Bioconjug. Chem.* **2010**, *21*, 1032–1042. [CrossRef] [PubMed]
23. Moon, S.-H.; Hong, M.K.; Kim, Y.J.; Lee, Y.-S.; Lee, D.S.; Chung, J.-K.; Jeong, J.M. Development of a Ga-68 labeled PET tracer with short linker for prostate-specific membrane antigen (PSMA) targeting. *Bioorg. Med. Chem.* **2018**, *26*, 2501–2507. [CrossRef] [PubMed]
24. Banerjee, S.R.; Pullambhatla, M.; Byun, Y.; Nimmagadda, S.; Green, G.; Fox, J.J.; Horti, A.; Mease, R.C.; Pomper, M.G. 68Ga-labeled inhibitors of prostate-specific membrane antigen (PSMA) for imaging prostate cancer. *J. Med. Chem.* **2010**, *53*, 5333–5341. [CrossRef] [PubMed]
25. Eder, M.; Schäfer, M.; Bauder-Wüst, U.; Hull, W.-E.; Wängler, C.; Mier, W.; Haberkorn, U.; Eisenhut, M. 68Ga-Complex Lipophilicity and the Targeting Property of a Urea-Based PSMA Inhibitor for PET Imaging. *Bioconjug. Chem.* **2012**, *23*, 688–697. [CrossRef] [PubMed]
26. Banerjee, S.R.; Pullambhatla, M.; Foss, C.A.; Nimmagadda, S.; Ferdani, R.; Anderson, C.J.; Mease, R.C.; Pomper, M.G. 64Cu-Labeled Inhibitors of Prostate-Specific Membrane Antigen for PET Imaging of Prostate Cancer. *J. Med. Chem.* **2014**, *57*, 2657–2669. [CrossRef] [PubMed]

27. Liu, W.; Hao, G.; Long, M.A.; Anthony, T.; Hsieh, J.T.; Sun, X. Imparting multivalency to a bifunctional chelator: A scaffold design for targeted PET imaging probes. *Angew. Chem. Int. Ed. Engl.* **2009**, *48*, 7346–7349. [CrossRef]
28. Harada, N.; Kimura, H.; Onoe, S.; Watanabe, H.; Matsuoka, D.; Arimitsu, K.; Ono, M.; Saji, H. Synthesis and Biologic Evaluation of Novel 18F-Labeled Probes Targeting Prostate-Specific Membrane Antigen for PET of Prostate Cancer. *J. Nucl. Med.* **2016**, *57*, 1978–1984. [CrossRef]
29. Ferro-Flores, G.; Luna-Gutiérrez, M.; Ocampo-García, B.; Santos-Cuevas, C.; Azorín-Vega, E.; Jiménez-Mancilla, N.; Orocio-Rodríguez, E.; Davanzo, J.; García-Pérez, F.O. Clinical translation of a PSMA inhibitor for ^{99m}Tc-based SPECT. *Nucl. Med. Biol.* **2017**, *48*, 36–44. [CrossRef]
30. Vallabhajosula, S.; Nikolopoulou, A.; Babich, J.W.; Osborne, J.R.; Tagawa, S.T.; Lipai, I.; Solnes, L.; Maresca, K.P.; Armor, T.; Joyal, J.L.; et al. ^{99m}Tc-Labeled Small-Molecule Inhibitors of Prostate-Specific Membrane Antigen: Pharmacokinetics and Biodistribution Studies in Healthy Subjects and Patients with Metastatic Prostate Cancer. *J. Nucl. Med.* **2014**, *55*, 1791–1798. [CrossRef]
31. Lutje, S.; Heskamp, S.; Cornelissen, A.S.; Poeppel, T.D.; van den Broek, S.A.; Rosenbaum-Krumme, S.; Bockisch, A.; Gotthardt, M.; Rijpkema, M.; Boerman, O.C. PSMA Ligands for Radionuclide Imaging and Therapy of Prostate Cancer: Clinical Status. *Theranostics* **2015**, *5*, 1388–1401. [CrossRef] [PubMed]
32. Kratochwil, C.; Giesel, F.L.; Stefanova, M.; Benešová, M.; Bronzel, M.; Afshar-Oromieh, A.; Mier, W.; Eder, M.; Kopka, K.; Haberkorn, U. PSMA-Targeted Radionuclide Therapy of Metastatic Castration-Resistant Prostate Cancer with 177Lu-Labeled PSMA-617. *J. Nucl. Med.* **2016**, *57*, 1170–1176. [CrossRef] [PubMed]
33. Pillai, M.R.A.; Dash, A.; Knapp, F.F. Sustained Availability of ^{99m}Tc: Possible Paths Forward. *J. Nucl. Med.* **2013**, *54*, 313–323. [CrossRef] [PubMed]
34. Kularatne, S.A.; Zhou, Z.; Yang, J.; Post, C.B.; Low, P.S. Design, synthesis, and preclinical evaluation of prostate-specific membrane antigen targeted (99m)Tc-radioimaging agents. *Mol. Pharm.* **2009**, *6*, 790–800. [CrossRef]
35. Lodhi, N.A.; Park, J.Y.; Kim, K.; Kim, Y.J.; Shin, J.H.; Lee, Y.-S.; Im, H.-J.; Jeong, J.M.; Khalid, M.; Cheon, G.J.; et al. Development of ^{99m}Tc-Labeled Human Serum Albumin with Prolonged Circulation by Chelate-then-Click Approach: A Potential Blood Pool Imaging Agent. *Mol. Pharm.* **2019**. [CrossRef]
36. Alberto, R.; Ortner, K.; Wheatley, N.; Schibli, R.; Schubiger, A.P. Synthesis and Properties of Boranocarbonate: A Convenient in Situ CO Source for the Aqueous Preparation of [^{99m}Tc$(OH_2)_3(CO)_3$]+. *J. Am. Chem. Soc.* **2001**, *123*, 3135–3136. [CrossRef]
37. Kasten, B.B.; Ma, X.; Liu, H.; Hayes, T.R.; Barnes, C.L.; Qi, S.; Cheng, K.; Bottorff, S.C.; Slocumb, W.S.; Wang, J.; et al. Clickable, Hydrophilic Ligand for fac-[M$(CO)_3$]+ (M = Re/^{99m}Tc) Applied in an S-Functionalized α-MSH Peptide. *Bioconjug. Chem.* **2014**, *25*, 579–592. [CrossRef]
38. Mizuno, Y.; Uehara, T.; Hanaoka, H.; Endo, Y.; Jen, C.-W.; Arano, Y. Purification-Free Method for Preparing Technetium-99m-Labeled Multivalent Probes for Enhanced in Vivo Imaging of Saturable Systems. *J. Med. Chem.* **2016**, *59*, 3331–3339. [CrossRef]
39. Lakić, M.; Sabo, L.; Ristić, S.; Savić, A.; Petričević, S.; Nikolić, N.; Vukadinović, A.; Janković, D.; Sabo, T.J.; Vranješ-Đurić, S. Synthesis and biological evaluation of ^{99m}Tc tricarbonyl complex of *O*,*O*′-diethylethylenediamine-*N*,*N*′-di-3-propanoate as potential tumour diagnostic agent. *Appl. Organomet. Chem.* **2016**, *30*, 81–88. [CrossRef]
40. Abrams, M.J.; Davison, A.; Jones, A.G.; Costello, C.E.; Pang, H. Synthesis and characterization of hexakis(alkyl isocyanide) and hexakis(aryl isocyanide) complexes of technetium(I). *Inorg. Chem.* **1983**, *22*, 2798–2800. [CrossRef]
41. Holman, B.L.; Jones, A.G.; Lister-James, J.; Davison, A.; Abrams, M.J.; Kirshenbaum, J.M.; Tumeh, S.S.; English, R.J. A new Tc-99m-labeled myocardial imaging agent, hexakis(*t*-butylisonitrile)-technetium(I) [Tc-99m TBI]: Initial experience in the human. *J. Nucl. Med.* **1984**, *25*, 1350–1355. [PubMed]
42. Doroudi, A.; Saraji, F.; Erfani, M.; Saadati, S.; Kisast, A.; Ahmadi, F.; Etesami, B. The stability of ^{99m}Tc-MIBI (Sestamibi) complex samples which prepared under ultrasound irradiation technique versus boiling water bath method. *J. Appl. Pharm. Sci.* **2016**, *6*, 126–134. [CrossRef]
43. Hao, G.Y.; Zang, J.Y.; Zhu, L.; Guo, Y.Z.; Liu, B.L. Synthesis, separation and biodistribution of ^{99m}Tc-CO-MIBI complex. *J. Label. Compd. Radiopharm.* **2004**, *47*, 513–521. [CrossRef]

44. Satpati, D.; Mallia, M.; Kothari, K.; Pillai, M.R.A. Comparative evaluation of $[^{99m}Tc(H_2O)_3(CO)_3]^+$ precursor synthesized by conventional method and by using carbonyl kit. *J. Label. Compd. Radiopharm.* **2004**, *47*, 657–668. [CrossRef]
45. Hao, G.; Zang, J.; Liu, B. Preparation and biodistribution of novel $^{99m}Tc(CO)_3$-CNR complexes for myocardial imaging. *J. Label. Compd. Radiopharm.* **2007**, *50*, 13–18. [CrossRef]
46. Duan, X.; Zhang, X.; Gan, Q.; Fang, S.A.; Ruan, Q.; Song, X.; Zhang, J. Novel ^{99m}Tc-labelled complexes with thymidine isocyanide: Radiosynthesis and evaluation as potential tumor imaging tracers. *MedChemComm* **2018**, *9*, 705–712. [CrossRef]
47. Lodhi, N.A.; Park, J.Y.; Hong, M.K.; Kim, Y.J.; Lee, Y.S.; Cheon, G.J.; Jeong, J.M. Development of (99m)Tc-labeled trivalent isonitrile radiotracer for folate receptor imaging. *Bioorg. Med. Chem.* **2019**. [CrossRef]
48. Barinka, C.; Byun, Y.; Dusich, C.L.; Banerjee, S.R.; Chen, Y.; Castanares, M.; Kozikowski, A.P.; Mease, R.C.; Pomper, M.G.; Lubkowski, J. Interactions between Human Glutamate Carboxypeptidase II and Urea-Based Inhibitors: Structural Characterization. *J. Med. Chem.* **2008**, *51*, 7737–7743. [CrossRef]
49. Kopka, K.; Benešová, M.; Bařinka, C.; Haberkorn, U.; Babich, J. Glu-Ureido–Based Inhibitors of Prostate-Specific Membrane Antigen: Lessons Learned During the Development of a Novel Class of Low-Molecular-Weight Theranostic Radiotracers. *J. Nucl. Med.* **2017**, *58*, 17S–26S. [CrossRef]
50. Liu, T.; Toriyabe, Y.; Kazak, M.; Berkman, C.E. Pseudoirreversible inhibition of prostate-specific membrane antigen by phosphoramidate peptidomimetics. *Biochemistry* **2008**, *47*, 12658–12660. [CrossRef]
51. Benešová, M.; Schäfer, M.; Bauder-Wüst, U.; Afshar-Oromieh, A.; Kratochwil, C.; Mier, W.; Haberkorn, U.; Kopka, K.; Eder, M. Preclinical Evaluation of a Tailor-Made DOTA-Conjugated PSMA Inhibitor with Optimized Linker Moiety for Imaging and Endoradiotherapy of Prostate Cancer. *J. Nucl. Med.* **2015**, *56*, 914–920. [CrossRef] [PubMed]
52. Wirtz, M.; Schmidt, A.; Schottelius, M.; Robu, S.; Gunther, T.; Schwaiger, M.; Wester, H.J. Synthesis and in vitro and in vivo evaluation of urea-based PSMA inhibitors with increased lipophilicity. *EJNMMI Res.* **2018**, *8*, 84. [CrossRef] [PubMed]
53. Wurzer, A.; Pollmann, J.; Schmidt, A.; Reich, D.; Wester, H.-J.; Notni, J. Molar Activity of Ga-68 Labeled PSMA Inhibitor Conjugates Determines PET Imaging Results. *Mol. Pharm.* **2018**, *15*, 4296–4302. [CrossRef] [PubMed]
54. Kuo, H.-T.; Pan, J.; Zhang, Z.; Lau, J.; Merkens, H.; Zhang, C.; Colpo, N.; Lin, K.-S.; Bénard, F. Effects of Linker Modification on Tumor-to-Kidney Contrast of 68Ga-Labeled PSMA-Targeted Imaging Probes. *Mol. Pharm.* **2018**, *15*, 3502–3511. [CrossRef] [PubMed]
55. Gorges, T.M.; Riethdorf, S.; von Ahsen, O.; Nastal, Y.P.; Rock, K.; Boede, M.; Peine, S.; Kuske, A.; Schmid, E.; Kneip, C.; et al. Heterogeneous PSMA expression on circulating tumor cells: A potential basis for stratification and monitoring of PSMA-directed therapies in prostate cancer. *Oncotarget* **2016**, *7*, 34930–34941. [CrossRef] [PubMed]
56. Hillier, S.M.; Kern, A.M.; Maresca, K.P.; Marquis, J.C.; Eckelman, W.C.; Joyal, J.L.; Babich, J.W. 123I-MIP-1072, a small-molecule inhibitor of prostate-specific membrane antigen, is effective at monitoring tumor response to taxane therapy. *J. Nucl. Med.* **2011**, *52*, 1087–1093. [CrossRef]
57. Hillier, S.M.; Maresca, K.P.; Lu, G.; Merkin, R.D.; Marquis, J.C.; Zimmerman, C.N.; Eckelman, W.C.; Joyal, J.L.; Babich, J.W. ^{99m}Tc-Labeled Small-Molecule Inhibitors of Prostate-Specific Membrane Antigen for Molecular Imaging of Prostate Cancer. *J. Nucl. Med.* **2013**, *54*, 1369–1376. [CrossRef]
58. Humblet, V.; Misra, P.; Bhushan, K.R.; Nasr, K.; Ko, Y.-S.; Tsukamoto, T.; Pannier, N.; Frangioni, J.V.; Maison, W. Multivalent scaffolds for affinity maturation of small molecule cell surface-binders and their application to prostate tumor targeting. *J. Med. Chem.* **2009**, *52*, 544–550. [CrossRef]
59. Yang, D.; Holt, G.E.; Velders, M.P.; Kwon, E.D.; Kast, W.M. Murine six-transmembrane epithelial antigen of the prostate, prostate stem cell antigen, and prostate-specific membrane antigen: Prostate-specific cell-surface antigens highly expressed in prostate cancer of transgenic adenocarcinoma mouse prostate mice. *Cancer Res.* **2001**, *61*, 5857–5860.
60. Schmittgen, T.D.; Zakrajsek, B.A.; Hill, R.E.; Liu, Q.; Reeves, J.J.; Axford, P.D.; Singer, M.J.; Reed, M.W. Expression pattern of mouse homolog of prostate-specific membrane antigen (FOLH1) in the transgenic adenocarcinoma of the mouse prostate model. *Prostate* **2003**, *55*, 308–316. [CrossRef]

61. Slusher, B.S.; Tsai, G.; Yoo, G.; Coyle, J.T. Immunocytochemical localization of the N-acetyl-aspartyl-glutamate (NAAG) hydrolyzing enzyme N-acetylated alpha-linked acidic dipeptidase (NAALADase). *J. Comp. Neurol.* **1992**, *315*, 217–229. [CrossRef] [PubMed]
62. Foss, C.A.; Mease, R.C.; Fan, H.; Wang, Y.; Ravert, H.T.; Dannals, R.F.; Olszewski, R.T.; Heston, W.D.; Kozikowski, A.P.; Pomper, M.G. Radiolabeled small-molecule ligands for prostate-specific membrane antigen: In vivo imaging in experimental models of prostate cancer. *Clin. Cancer Res. Off. J. Am. Assoc. Cancer Res.* **2005**, *11*, 4022–4028. [CrossRef] [PubMed]
63. Bacich, D.J.; Pinto, J.T.; Tong, W.P.; Heston, W.D. Cloning, expression, genomic localization, and enzymatic activities of the mouse homolog of prostate-specific membrane antigen/NAALADase/folate hydrolase. *Mamm. Genome* **2001**, *12*, 117–123. [CrossRef] [PubMed]
64. Kelly, J.; Amor-Coarasa, A.; Ponnala, S.; Nikolopoulou, A.; Williams, C.; Schlyer, D.; Zhao, Y.; Kim, D.; Babich, J.W. Trifunctional PSMA-targeting constructs for prostate cancer with unprecedented localization to LNCaP tumors. *Eur. J. Nucl. Med. Mol. Imaging* **2018**. [CrossRef] [PubMed]
65. Yang, P.-Y.; Wu, H.; Lee, M.Y.; Xu, A.; Srinivasan, R.; Yao, S.Q. Solid-Phase Synthesis of Azidomethylene Inhibitors Targeting Cysteine Proteases. *Org. Lett.* **2008**, *10*, 1881–1884. [CrossRef]
66. Skwarecki, A.S.; Skarbek, K.; Martynow, D.; Serocki, M.; Bylińska, I.; Milewska, M.J.; Milewski, S. Molecular Umbrellas Modulate the Selective Toxicity of Polyene Macrolide Antifungals. *Bioconjug. Chem.* **2018**, *29*, 1454–1465. [CrossRef]
67. Lazarova, N.; James, S.; Babich, J.; Zubieta, J. A convenient synthesis, chemical characterization and reactivity of $[Re(CO)_3(H_2O)_3]Br$: The crystal and molecular structure of $[Re(CO)_3(CH_3CN)_2Br]$. *Inorg. Chem. Commun.* **2004**, *7*, 1023–1026. [CrossRef]